

# An active Distribution Network Equivalent derived from large-disturbance Simulations with Uncertainty

Gilles Chaspierre, *Student Member, IEEE*, Guillaume Denis, *Member, IEEE*,  
Patrick Panciatichi *Fellow Member, IEEE* and Thierry Van Cutsem, *Fellow Member, IEEE*

**Abstract**—A reduced-order, “grey-box” model of an active distribution network, intended for dynamic simulations of the transmission system, is derived. The network hosts inverter-based generators as well as static and motor loads, whose dynamic parameters are affected by uncertainty. This issue is addressed using Monte-Carlo simulations. The parameters of the equivalent are adjusted to match as closely as possible the average of the randomized responses, while their dispersion is accounted for through the weights of the weighted least-square minimization. A procedure is used to remove from the identification the parameters with negligible impact. To avoid over-fitting, the equivalent is tuned for multiple large-disturbance simulations. A recursive procedure is used to select the smallest possible subset of disturbances involved in the least-square minimization. Simulation results with a 75-bus MV test-system are reported. They show that the equivalent is able to reproduce with good accuracy the discontinuous controls of inverter-based generators, such as reactive current injection and tripping.

**Index Terms**—active distribution network, inverter-based generator, dynamic equivalent, grey-box model, uncertain dynamic model, Monte-Carlo simulations, LASSO method.

## I. INTRODUCTION

**D**ISTRIBUTION systems are getting more and more complex owing to the increasing number of Inverter-Based Generators (IBGs) connected at Medium-Voltage (MV) level. This makes distribution networks more and more responsive and their influence on the whole power system dynamics increases. Therefore, it becomes important for Transmission System Operators (TSOs) to model those Active Distribution Networks (ADNs) in their dynamic simulation studies. However, time simulations of combined transmission and distribution systems are impractical owing to large computing times and heavy maintenance of the model. Moreover, in some countries, confidentiality rules prevent Distribution System Operators (DSOs) from sharing detailed data with TSOs. To tackle both issues, it makes sense to use equivalents, i.e. reduced-order models of the ADNs in dynamic simulations of the transmission system. This, in turn, requires the equivalent to show a good compromise between accuracy and simplicity.

The approaches for setting up equivalents can be classified into measurement-based and simulation-based. The former use measurements (of typically the power flow into the ADN) to best tune the parameters of the reduced-order model (e.g. [1],

[2],[3]). The focus in this paper is on large disturbances, such as faults, taking place in the transmission system. Measurements of the ADN response to such events are little available and, if they are, the number of events is too limited for identifying an equivalent valid for other disturbances. Hence, a simulation-based approach is considered in this paper.

The first step consists of setting up a detailed, i.e. unreduced model of the ADN. While it can be generally assumed that the network model is accurate, dynamic models on the other hand, are affected by uncertainty. For instance, in load models, the parameters of equivalent motors are usually set to “typical” values (e.g. [4]) to account for a population of similar smaller motors. Regarding IBGs, grid codes allow for a range of permissible behaviours [5], [6]. Monte-Carlo (MC) simulations are a traditional way to deal with such uncertainties [7]. For a given disturbance, dynamic responses are generated for randomized variations of the uncertain parameters [8]. Statistics such as the average (or the median) and the standard deviations provide useful information on the time-varying impact of parameter uncertainty.

The second step consists of deriving a reduced-order model. A recent review of dynamic equivalents to reproduce the response of loads and ADNs can be found in [9].

“Black-box” approaches have been proposed, e.g. in [2], [3]. They are suitable when no model of the ADN is available. In this case, the parameters are identified from measurements, with the already mentioned limitation in terms of events.

Instead, this paper deals with a reduced model of the “grey-box” type, as recommended in [10] and [11]. Such an equivalent is usually appealing for it involves components of the type used in the unreduced system. While its mathematical model is specified, the involved parameters have to be identified. Examples of grey-box model identification of ADNs can be found in [12]-[17]. However, no attention has been paid to the above-mentioned uncertainty affecting the ADN model parameters. Furthermore, the proposed models do not reproduce the discontinuous response of IBGs, in particular the tripping of some of them. This is another aspect covered in this paper.

The unreduced and the equivalent ADN models assume a balanced three-phase distribution grid and are used in dynamic simulations under the phasor approximation [18]. The equivalent must be able to reproduce with good accuracy the nonlinear behaviour of the system and in particular the discontinuous controls of IBGs, such as reactive current injection, active current recovery and tripping.

A standard identification procedure consists of adjusting the

G. Chaspierre is with the Dept. of Elec. Eng. and Comp. Science, University of Liège, Belgium, e-mail: g.chaspierre@uliege.be.

G. Denis and P. Panciatichi are with the Research & Development Dept., RTE, Paris La Défense, France, e-mail: guillaume.denis@rte-france.com.

T. Van Cutsem is with the Fund for Scientific Research (FNRS) at the University of Liège, Belgium, e-mail: t.vancutsem@uliege.be.

parameters to approach in the least-square sense the response of the unreduced system. In order to account for uncertainty, the approach considered in this paper consists of: (i) using the average of the randomized MC simulations as reference, and (ii) weighting the deviations with respect to the latter to account for the dispersion observed in MC simulations.

The number of parameters to adjust should be kept “as small as possible”, to make the least-square minimization less demanding, but also the parameter values more consistent from one case to another and, hence, easier to interpret [19]. To that purpose, a method inspired of the Least Absolute Shrinkage and Selection Operator (LASSO) is proposed in this paper to discard from the identification the parameters with a negligible impact. The original LASSO method was proposed for linear regression and presented in [20]. A nonlinear variant has been used in [21], [22] to identify power system models.

Another distinctive feature of the procedure presented in this paper is the training of the equivalent from multiple disturbances (in the transmission system). The main objective is to avoid over-fitting one particular scenario. Since handling numerous disturbances can be demanding, a recursive procedure is proposed to select the smallest possible subset of disturbances, from which the parameters are identified. The procedure guarantees the accuracy of the equivalent with respect to disturbances not involved in the training.

This paper builds on the authors’ previous work (e.g. [23]). The novelties are : (i) a different structure of the equivalent, (ii) an improved training procedure, (iii) the handling of IBG tripping, (iv) the identification of significant parameters, (v) simulation results from a more complex test system.

The rest of the paper is organized as follows. The unreduced and reduced ADN models are described in Section II and III, respectively. Section IV details the optimization of the reduced model parameters. Simulation results are reported in Section V, and conclusions are offered in Section VI.

## II. UNREDUCED MODEL OF THE ADN

The ADN model aims at rendering the impact on transmission system dynamics of numerous loads and IBGs dispersed in a distribution grid. Rotor angle, frequency and voltage stability studies are targeted. The focus is on transients lasting up to 10 to 20 seconds after a large disturbance, but features relevant to long-term dynamics can be easily added.

The model used for, respectively, all loads and all IBGs is outlined in this section. Note that the methodology easily accommodates other load components (e.g. [10], [18]) and other types of dispersed generators (e.g. synchronous machines).

### A. Load model

The generic load model considered is depicted in Fig. 1. It is split into a standard exponential model and a third-order induction motor [18]. Initially, the motor consumes a fraction  $m$  of the total active power and the compensation capacitor is adjusted to satisfy a specified power factor  $\cos \phi_m$ .

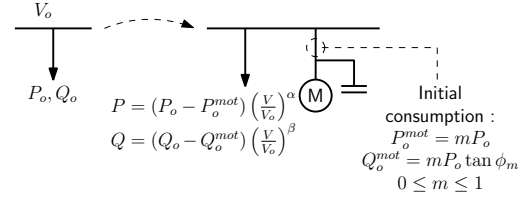


Fig. 1. Load model: decomposition into exponential and motor parts

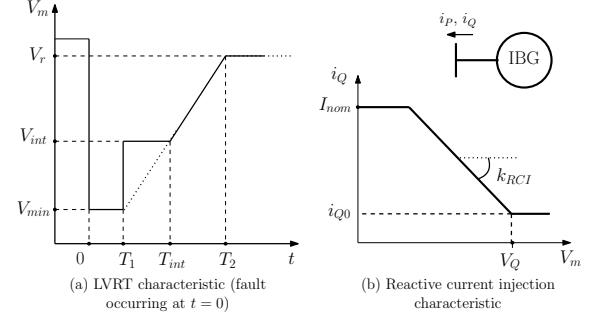


Fig. 2. Controls of the IBG in response to large voltage deviations

### B. IBG model

A generic IBG model is considered, aimed at capturing the variations of the injected current with the terminal voltage. The embedded controls meet recent grid code requirements (e.g. [5], [6]), as detailed hereafter. The model is described in greater detail in [24].

1) *Phase Locked Loop (PLL)*: The PLL estimates the phase angle of the terminal voltage, in order to inject the current with the proper phase angle with respect to that voltage. A Proportional-Integral (PI) control is used to align the  $d$  axis with the voltage phasor; the PLL response time is not neglected.

2) *Low Voltage Ride-Through (LVRT)*: Grid codes request IBGs above a given rating to remain connected to the grid in low voltage conditions. Yet the units are allowed to disconnect if their terminal voltage falls below an LVRT curve. The curve implemented is defined by six parameters, as shown in Fig. 2.a.

3) *Reactive current injection*: Grid codes request large-capacity IBGs to inject reactive current into the grid if their terminal voltage falls below some threshold. That current varies linearly with the measured voltage, as shown in Fig. 2.b where  $i_{Q0}$  is the initial reactive current,  $I_{nom}$  the IBG nominal current and  $V_m$  the measured terminal voltage.

4) *Current limit*: In low voltage conditions, in order to leave room for the reactive current without exceeding the  $I_{nom}$  limit, the active current is decreased. For a large enough voltage drop, it may even be decreased to zero.

5) *Rate of active current recovery*: After fault clearing, once the voltage has recovered to normal values, the IBG active current recovers. The recovery cannot be too fast to prevent fast dynamics that can de-stabilize the system, but not too slow either to avoid long lasting power imbalance. The value of the rate of recovery of the active current has been chosen in the range given in [25].

6) *Other features*: The model also involves time constants affecting the voltage measurement and the outer control loops.

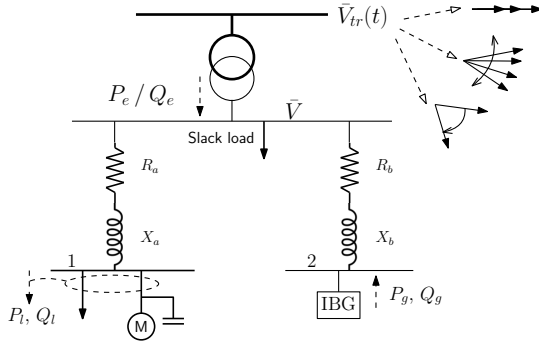


Fig. 3. Structure of ADN equivalent

### III. REDUCED (EQUIVALENT) ADN MODEL

#### A. Structure of the equivalent

The structure of the equivalent is shown in Fig. 3.

The connection to the transmission grid is through a single transformer, which is retained in the equivalent. The distributed IBGs (resp. loads) of the original system are lumped into one aggregated IBG (resp. load). The aggregated load and the aggregated IBG are connected through distinct impedances  $R_a + jX_a$  and  $R_b + jX_b$  to take account their different distributions within the ADN.

Note that the methods presented in this paper apply to other structures of the equivalent, as discussed in Appendix A.

#### B. Load and IBG model in the equivalent

The model used for the aggregated load in the equivalent is the same as that of individual loads in the unreduced system (see Section II-A).

Similarly, the model used for the aggregated IBG retains the features of the model of individual IBGs in the unreduced system (see Section II-B). However, instead of the LVRT feature, the aggregated model must account for the possible tripping of *some* IBGs in the unreduced system [24], [27]. Indeed, the voltages being different from one IBG bus to another, during a fault, some units may trip while the others remain connected. Since there is a single aggregated IBG, the aforementioned situation is accounted by providing the aggregated IBG with a “partial tripping” feature, as illustrated in Fig. 4. It consists of multiplying the output current  $\bar{I}_{nt}$  given by the model without tripping by a factor  $f$  ( $0 < f < 1$ ) evolving as depicted in the right part of Fig. 4. When the voltage  $V$  of the equivalent IBG falls below the  $V_{pt}$  threshold,  $f$  drops to  $\gamma$ , which corresponds to losing a fraction  $1 - \gamma$  of the IBGs. For further voltage drops,  $f$  decreases linearly with  $V$ . Full disconnection ( $f = 0$ ) takes place for  $V = V_{ft}$ . If  $V$  recovers before reaching  $V_{ft}$  (as shown in Fig. 4)  $f$  remains at the  $f_{min}$  value corresponding to the voltage nadir. Thus, the tripping that could take place after the voltage nadir is not considered. The technique is a simplified version of the one considered in [24] and similar to the one used in [27].

#### C. Parameters to identify

The 20 parameters to identify are (see Figs. 1, 2 and 4) :

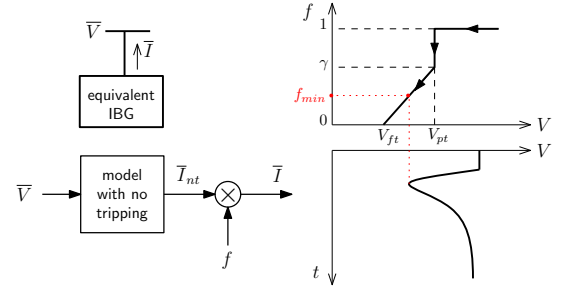


Fig. 4. “Partial tripping” feature of the aggregated IBG

- for the aggregated load :  $\alpha$  and  $\beta$  in the exponential model and, for the motor, the stator and rotor resistances, the magnetizing and the two leakage reactances, the inertia constant and the nominal apparent power;
- for the aggregated IBG : the nominal current, the rate of recovery of the active current,  $k_{RCI}$  and  $V_Q$  (reactive current injection),  $\gamma$ ,  $V_{pt}$  and  $V_{ft}$  (partial tripping);
- for the equivalent impedances :  $R_a$ ,  $R_b$ ,  $X_a$  and  $X_b$ .

#### D. Initialization

The active power  $P_l$  and reactive power  $Q_l$  initially consumed by the aggregated load (see Fig. 3) are obtained by summing the individual load powers throughout the ADN. Similarly,  $P_g$  and  $Q_g$  are obtained by summing the powers produced by the dispersed IBGs.

The initial input powers  $P_e$  and  $Q_e$ , which include the losses in the equivalent impedances  $R_a + jX_a$  and  $R_b + jX_b$ , may not match the powers estimated by the TSO. Furthermore, in the course of identifying the parameters of the equivalent,  $P_e$  and  $Q_e$  are specified but  $R_a$ ,  $R_b$ ,  $X_a$  and  $X_b$  vary. In both cases, a “slack” load is added at the MV end of the transformer. Usually small, this load is treated as constant admittance.

### IV. REDUCED MODEL IDENTIFICATION

As mentioned in the Introduction, a number  $d$  of disturbances are used to train the equivalent in order to avoid over-fitting one particular scenario. Each of them consists of imposing large variations of the amplitude, the phase angle, or the frequency of the voltage source  $\bar{V}_{tr}$  replacing the transmission system (see Fig. 3).

#### A. Monte-Carlo simulations

It is assumed that the dynamic models of loads and IBGs are qualitatively correct but involve uncertain parameters. MC simulations are used to assess the impact of this uncertainty on the dynamic response of the unreduced system.

Assume that the ADN feeds  $n_L$  loads and hosts  $n_G$  IBGs. Let  $\pi_L$  and  $\pi_G$  be the number of uncertain parameters in the load and IBG models, respectively. For the whole system, those parameters are gathered in a vector  $\mathbf{p}$  with  $n_L\pi_L + n_G\pi_G$  components. The latter are treated as independent random variables, and  $\mathbf{p}$  is uniformly distributed in  $[\mathbf{p}^{min} \mathbf{p}^{max}]$ . By so doing, the parameters are randomized from one MC simulation to another but also from one load (resp. one IBG) to another.

In the absence of further information, uniform distributions are considered for the randomized parameters. Appendix B offers a comparison with Gaussian distributions.

Let  $s$  be the number of randomly drawn instances of  $\mathbf{p}$ .

The variables of interest are the active and reactive power entering the ADN. For the  $j$ -th disturbance ( $j = 1, \dots, d$ ), the  $i$ -th instance  $\mathbf{p}^{(i)}$  of  $\mathbf{p}$  ( $i = 1, \dots, s$ ) and a discrete time instant  $k$ , the following values are extracted from the MC simulations:

- $P(j, k, \mathbf{p}^{(i)})$  the active power at time  $k$  obtained with  $\mathbf{p}^{(i)}$
- $Q(j, k, \mathbf{p}^{(i)})$  the corresponding reactive power
- $\mu_P(j, k)$  the average of the  $s$  values  $P(j, k, \mathbf{p}^{(i)})$
- $\mu_Q(j, k)$  the average of the  $s$  values  $Q(j, k, \mathbf{p}^{(i)})$
- $\sigma_P(j, k)$  the standard deviation of the  $s$  values  $P(j, k, \mathbf{p}^{(i)})$
- $\sigma_Q(j, k)$  the standard deviation of the  $s$  values  $Q(j, k, \mathbf{p}^{(i)})$ .

### B. Weighted least-square identification

The equivalent is tuned so that its responses to disturbances matches the average response of the unreduced system.

The parameters to identify are grouped in a vector  $\boldsymbol{\theta}$ . The latter is adjusted so that, for each discrete time  $k$  and for all disturbances  $j$ , the active power  $P_e(\boldsymbol{\theta}, j, k)$  (resp. the reactive power  $Q_e(\boldsymbol{\theta}, j, k)$ ) entering the equivalent approaches in the least square sense the average  $\mu_P(j, k)$  (resp.  $\mu_Q(j, k)$ ).

Thus the following constrained optimization is considered :

$$\min_{\boldsymbol{\theta}} F(\boldsymbol{\theta}) = \frac{1}{d} \sum_{j=1}^d [F_P(\boldsymbol{\theta}, j) + F_Q(\boldsymbol{\theta}, j)] \quad (1)$$

$$\text{with } F_P(\boldsymbol{\theta}, j) = \frac{1}{N} \sum_{k=1}^N \left[ \frac{P_e(\boldsymbol{\theta}, j, k) - \mu_P(j, k)}{\sigma_P(j, k)} \right]^2 \quad (2)$$

$$F_Q(\boldsymbol{\theta}, j) = \frac{1}{N} \sum_{k=1}^N \left[ \frac{Q_e(\boldsymbol{\theta}, j, k) - \mu_Q(j, k)}{\sigma_Q(j, k)} \right]^2 \quad (3)$$

$$\boldsymbol{\theta}^L \leq \boldsymbol{\theta} \leq \boldsymbol{\theta}^U \quad (4)$$

where  $N$  is the number of discrete times of the simulation. The bounds  $\boldsymbol{\theta}^L$  and  $\boldsymbol{\theta}^U$  keep  $\boldsymbol{\theta}$  in realistic ranges of values.

Note that each term in (2) (resp. (3)) is weighted by the inverse of the variance  $\sigma_P^2(j, k)$  (resp.  $\sigma_Q^2(j, k)$ ) to reflect the dispersion of the MC responses. By so doing, at a given time  $k$ , the deviation from  $\mu_P(j, k)$  (resp.  $\mu_Q(j, k)$ ) is more penalized if the dispersion of the power response in the MC simulations is small. Conversely, at a time  $k$  when a large dispersion is observed, denoting a large impact of parameter uncertainty, the deviation of the equivalent from  $\mu_P(j, k)$  (resp.  $\mu_Q(j, k)$ ) is less penalized. If  $\sigma_P(j, k)$  or  $\sigma_Q(j, k)$  becomes too small, the subsequent times  $k$  are not included in (2),(3) to avoid distorting the minimization.

### C. Solving the optimization problem (1)-(4)

An analytical expression of the gradient of the objective function (1) being impossible to derive, standard mathematical programming methods cannot be envisaged to solve the least-square minimization problem (1)-(4). Instead, a metaheuristic, derivative-free optimization method has been preferred. Among the wide variety of metaheuristic methods an evolutionary algorithm, namely Differential Evolution (DE) [28]

has been preferred. The choice of DE was motivated by the comparison reported in [29], where it outperformed other algorithms on various benchmark problems. A systematic comparison with other methods - such as those used in [30], [31], [32], [33] - was outside the scope of this research. While other algorithms could offer a most welcome speed-up, DE has been found to be a reliable solver for the optimization problem (1)-(4) in a large number of cases.

The solver has been derived from the open source Python code available in [34]. The version of the algorithm is denoted *rand/1/bin* because  $\boldsymbol{\theta}$  is randomly chosen and only one vector difference is added to it. The binomial crossover strategy was used to mix the information of the trial and the target vectors. Moreover, at each new generation, the mutation factor is randomly selected in the range [0.5, 1] as it has been found that this technique may improve convergence significantly [28]. More information is available in [34].

Since the DE algorithm is iterative, a proper stopping criterion is important. It was found appropriate to stop iterating when, for all disturbances ( $j = 1, \dots, d$ ) :

$$F_P(\boldsymbol{\theta}, j) \leq 1 \quad \text{and} \quad F_Q(\boldsymbol{\theta}, j) \leq 1 \quad (5)$$

i.e. when the deviation of  $P_e(\boldsymbol{\theta}, j, k)$  from  $\mu_P(j, k)$  (resp.  $Q_e(\boldsymbol{\theta}, j, k)$  from  $\mu_Q(j, k)$ ) is smaller than  $\sigma_P(j, k)$  (resp.  $\sigma_Q(j, k)$ ) on average over discrete times  $k$ . Yet a maximum number of DE iterations is enforced in case (5) is not satisfied.

### D. Recursive training procedure

The larger the number  $d$  of disturbances, the lower the risk to over-fitting but the larger the computational burden to solve the minimization problem (1)-(4). To tackle this problem, a recursive procedure is proposed, which consists of focusing on a subset of disturbances from which the parameters are identified. More precisely, "training" disturbances are progressively added, until the equivalent is found sufficiently accurate with respect to all other, non-trained disturbances. The detailed procedure is as follows :

- 1) A set of  $c$  candidate disturbances is initially defined. For each disturbance, MC simulations are performed and the time-varying averages  $\mu_P(j, k)$ ,  $\mu_Q(j, k)$  and standard deviations  $\sigma_P(j, k)$ ,  $\sigma_Q(j, k)$  are collected.
- 2) A small subset of disturbances is selected for the initial training :  $d := d_0 \ll c$ .
- 3) The minimization problem (1)-(4) is solved, with the stopping criterion (5), yielding the solution  $\hat{\boldsymbol{\theta}}$ . The following worst scores are determined :

$$F_P^{max}(\hat{\boldsymbol{\theta}}) = \max_{j=1, \dots, d} F_P(\hat{\boldsymbol{\theta}}, j) \quad (6)$$

$$F_Q^{max}(\hat{\boldsymbol{\theta}}) = \max_{j=1, \dots, d} F_Q(\hat{\boldsymbol{\theta}}, j) \quad (7)$$

- 4) With that value  $\hat{\boldsymbol{\theta}}$ , the scores  $F_P(\hat{\boldsymbol{\theta}}, i)$  and  $F_Q(\hat{\boldsymbol{\theta}}, i)$  are computed for each non-trained disturbance  $i$ .
- 5) If, for all of them :

$$F_P(\hat{\boldsymbol{\theta}}, i) \leq \max(1, F_P^{max}(\hat{\boldsymbol{\theta}})) \quad (8)$$

$$F_Q(\hat{\boldsymbol{\theta}}, i) \leq \max(1, F_Q^{max}(\hat{\boldsymbol{\theta}})), \quad (9)$$

then, the procedure stops; else, the disturbance with the largest value of  $F_P(\hat{\theta}, i)$  is added to the training set and similarly for the one with the largest value of  $F_Q(\hat{\theta}, i)$ , unless it is the same disturbance.  $d$  is increased by 1 or 2, accordingly.

- 6) Steps 3 to 5 are repeated using the last value  $\hat{\theta}$  as initial guess in the minimization.

The right-hand side in (8) and (9) is justified as follows. If the worst scores of the trained disturbances do not satisfy the tolerance of 1 specified in (5), that tolerance is also relaxed for the non-trained disturbances.

### E. Discarding non significant parameters

As mentioned in the Introduction, a procedure that bears the spirit of the LASSO method is used to discard the less significant parameters of the least-square minimization, for higher computational efficiency, better consistency and easier interpretation of the results.

The method consists of adding a penalty term to (1) :

$$\min_{\theta} F(\theta) + \lambda \sum_{l=1}^n |\theta_l^{ref} - \theta_l| \quad (10)$$

where  $\lambda$  is a scaling factor,  $n$  is the size of  $\theta$  and  $\theta^{ref}$  is a reference value for the parameters. The penalty term tends to make  $\theta_l$  depart from its  $\theta_l^{ref}$  reference only if this yields a significant decrease of  $F(\theta)$ , i.e. if  $\theta_l$  has a significant influence on  $F(\theta)$ , thereby making the dynamic response of the equivalent more accurate.

The procedure starts with  $\lambda$  set to a large value  $\lambda_o$ , which yields  $\hat{\theta} \simeq \theta^{ref}$ . Then,  $\lambda$  is decreased steps by steps (namely divided by an integer  $a$  larger than one at each step). For each value, the minimization problem (1)-(4) is solved with the penalty term added as in (10). This procedure is repeated until the accuracy condition (5) is satisfied.

At this point, the components of  $\hat{\theta}$  and  $\theta^{ref}$  are compared. For the  $l$ -th component ( $l = 1, \dots, n$ ), if :

$$\frac{|\hat{\theta}_l - \theta_l^{ref}|}{\theta_l^{ref}} \leq \delta \quad (11)$$

the parameter of concern is considered to have little impact, since constraining  $\theta_l$  to remain close to its reference  $\theta_l^{ref}$  has little impact on the final scores  $F_P(\hat{\theta}, j)$  and  $F_Q(\hat{\theta}, j)$ .

A non significant parameter is given the estimated value (i.e.  $\theta_l = \hat{\theta}_l$ ), and is removed from  $\theta$ .

For the significant parameters, the estimated value  $\hat{\theta}_l$  is used to update the limits in (4) :

$$\theta_l^L = \hat{\theta}_l - \alpha \hat{\theta}_l \quad (12)$$

$$\theta_l^U = \hat{\theta}_l + \alpha \hat{\theta}_l \quad (13)$$

where  $0 \leq \alpha \leq 1$ . The recursive procedure of Section IV-D is then applied with the original objective function (1).

*Remark.* It may happen that a parameter  $\theta_l$  impacts the dynamic response of the equivalent, but remains close to its reference value  $\theta_l^{ref}$ , because the latter happens to be near optimal. Therefore, it would be more accurate to state that the method identifies parameters whose variations from

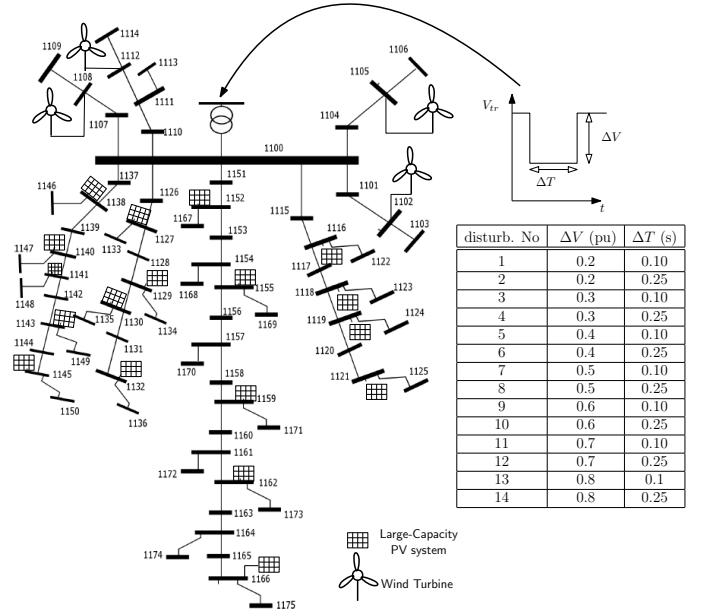


Fig. 5. One-line diagram of test system and candidate training disturbances

their reference values improve the dynamic response of the equivalent. Even if a parameter  $\theta_l$  is unduly labeled as non significant, this has no consequence on accuracy since it is set to its near optimal value  $\theta_l^{ref}$ .

## V. SIMULATION RESULTS

### A. Test system and disturbances

The simulations have been performed on a modified version of the 75-bus 11-kV distribution system previously used in [13]. Its one-line diagram is given in Fig. 5. In total, the system hosts 22 dispersed IBGs, belonging to two categories : large-capacity PhotoVoltaic (PV) systems and Wind Turbines (WTs). WTs are located closer to the main substation. All IBGs have fault-ride through and reactive current injection capabilities. Their total capacity is 14.8 MW. The initial IBG production is 9.8 MW. The WTs operate at 80 % of their capacity, and the PV units at 50 % of their capacity. The loads are connected to the (75-22=) 53 buses without IBGs. The total initial consumption is 19.95 MW / 3.40 Mvar. The net power entering the system is 10.33 MW / 3.63 Mvar.

Extensive simulation results have shown that the equivalent trained from voltage dips properly covers other types of disturbances, such as phase jumps, voltage oscillations or frequency variations. This will be illustrated in Section V-H. The reverse is not true. The candidate training disturbances are thus voltage dips. They are listed in Fig. 5. They are characterized by a depth  $\Delta V$  and a duration  $\Delta T$  typical of fault clearing by (main and back-up) protections at transmission level.

The dynamic evolutions of the active power  $P$  and reactive power  $Q$  entering the ADN are collected over five seconds. The RAMSES software for dynamic simulation in phasor mode has been used [35]; the average time step size is 0.01 s.

### B. MC simulations of the unreduced system

The parameters randomized in the MC simulations are :

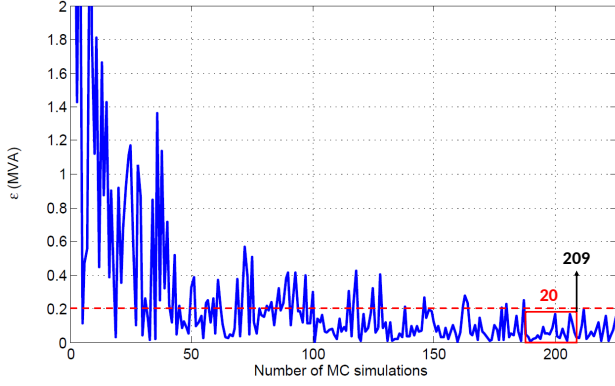


Fig. 6. Evolution of  $\varepsilon$  with  $s$  (14 disturbances)

- for the motor part of each load : the stator and rotor resistances, the magnetizing and the two leakage reactances, the inertia constant, the fraction of quadratic mechanical torque, the load factor [4], the fraction  $m$  of the power initially consumed by the motor and the initial power factor  $\cos \phi_m$  (see Fig. 1);
- for the static part of each load : the exponents  $\alpha$  and  $\beta$  (see Fig. 1);
- for each IBG : the rate of active current recovery, the time constants of the PLL and the power controllers [24], the  $k_{RCI}$  slope and  $V_Q$  voltage (see Fig. 2(b)).

One practical issue is to select the number  $s$  of MC simulations. This is a compromise between representativity of the sample and computational burden. Keeping in mind that the purpose is to extract the reference values  $\mu_P$  and  $\mu_Q$  used in (2),(3), MC simulations can be stopped when those values do no longer vary significantly with  $s$  [8]. This is decided by monitoring :

$$\varepsilon = \sqrt{\varepsilon_P^2 + \varepsilon_Q^2} \quad (14)$$

$$\text{with } \varepsilon_P^2 = \frac{1}{dn} \sum_{j=1}^d \sum_{k=1}^n \left[ \mu_P^{(s+1)}(j, k) - \mu_P^{(s)}(j, k) \right]^2 \quad (15)$$

$$\varepsilon_Q^2 = \frac{1}{dn} \sum_{j=1}^d \sum_{k=1}^n \left[ \mu_Q^{(s+1)}(j, k) - \mu_Q^{(s)}(j, k) \right]^2 \quad (16)$$

where  $\mu_P^{(s)}(j, k)$  is the value of  $\mu_P(j, k)$  computed over the first  $s$  MC simulations, and similarly for reactive power.

An example of variation of  $\varepsilon$  with  $s$  is given in Fig. 6. MC simulations are stopped when  $\varepsilon$  remains smaller than 0.2 MVA for 20 successive values of  $s$ . As shown in the figure, this yields  $s = 209$ .

The value of  $\varepsilon$  is a compromise between representativity of the sample and computational burden. For instance, when decreasing  $\varepsilon$  to 0.15 MVA (resp. 0.1 MVA)  $s$  increases to 260 (resp. 320). The corresponding time evolutions of  $\mu_P$  and  $\mu_Q$  are shown in Fig. 7), relative to disturbance No. 7. There is clearly no gain of accuracy in setting  $\varepsilon$  lower than 0.2 MVA.

Figure 8 shows the 209 randomized time evolutions of  $P$  and  $Q$  in response to disturbance No. 7. All curves start from the same value, since the same operating point is considered,

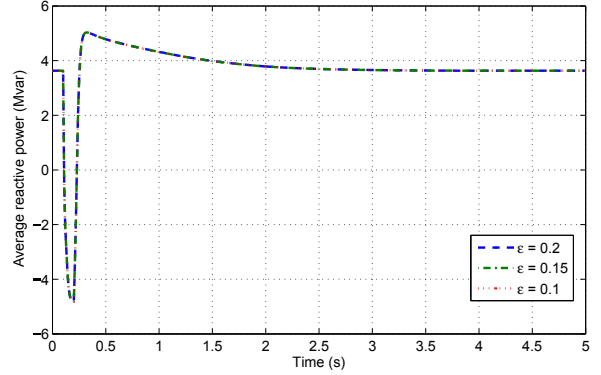
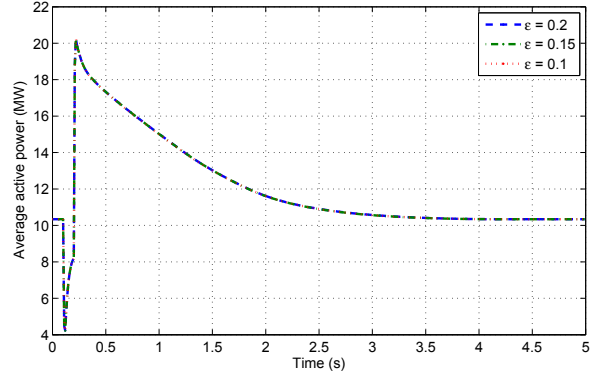


Fig. 7. Evolution of  $\mu_P$  and  $\mu_Q$  for different values of  $\varepsilon$ ; disturbance #7

and come back to that value, since this rather mild disturbance does not trigger IBG disconnection.

The overall evolution is explained as follows. During the voltage dip, the load with exponential model decreases while the IBGs sacrifice their active current to inject reactive current. This is confirmed by the lower plot in Fig. 8, where the reactive power flow reverses during the voltage dip. When the voltage recovers to its initial value, so do the powers of loads with exponential model, while the motors draw some additional power, due to their re-acceleration. Moreover, the IBGs ramp up their active power. This takes between 1.8 and 3.8 s to the various IBGs.

Figure 8 also shows the distribution of power values at  $t = 0.5$  s with the corresponding values of  $\mu_P, \sigma_P, \mu_Q$  and  $\sigma_Q$ . There are no “outliers” in the set of system responses. This justifies using the average for  $\mu_P$  and  $\mu_Q$ . If outliers were present, the median would provide a more robust estimate.

Another source of uncertainty stems from the LVRT capability of individual IBGs. Grid codes state that they *are allowed* to disconnect if their voltages fall below the LVRT curve, but *do not request* their disconnection. This has been taken into account by also randomizing the disconnection of IBGs in the MC simulations : among the IBGs with voltage falling below the LVRT curve, some disconnect, some do not.

Figure 9 shows the 209 evolutions of  $P$  and  $Q$  in response to the more severe disturbance No. 13. The large dispersion of final values results from the random disconnection of IBGs.

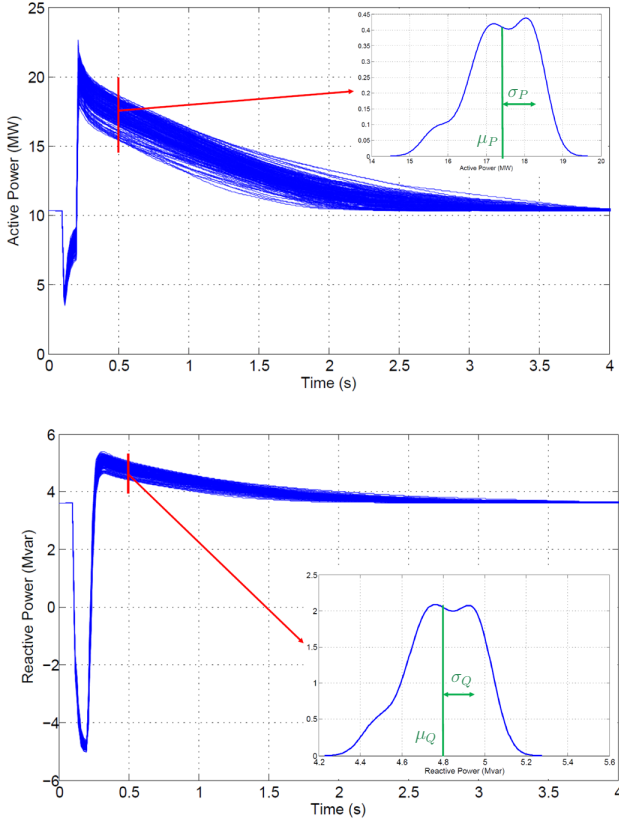


Fig. 8. Randomized evolutions of  $P$  and  $Q$  in response to disturbance # 7

### C. Steps of the reduced model identification

The bounds  $\theta^L$  and  $\theta^U$  of the search interval in (4) have been set to plausible values of the corresponding parameters, inspired of literature (e.g. [4]) or grid codes.

The equivalent impedances  $R_a + jX_a$  and  $R_b + jX_b$  have been first estimated using a network reduction technique. Then, the DE algorithm is let to adjust  $R_a, X_a, R_b$  and  $X_b$  in intervals centered on the so obtained estimates.

The equivalent is identified in three steps :

- 1) scenarios without IBG disconnection have been considered, leaving aside  $\gamma, V_{pt}$  and  $V_{ft}$  (see Fig. 4). Among the  $(20-3=)$  17 remaining parameters, 10 have been identified as significant by the method of Section IV-E;
- 2) those 10 parameters have been optimized by the recursive training algorithm of Section IV-D;
- 3) scenarios with IBG disconnection have been used to identify  $\gamma, V_{pt}$  and  $V_{ft}$ , the previous 10 parameters being set to their values found at Step 2).

### D. Step 1 : Identifying the significant parameters

The LASSO method has been used on disturbances No. 7 and 8 with intermediate values of the voltage dip (see Fig. 5).  $\theta^{ref}$  has been set to  $(\theta^L + \theta^U)/2$ .

Figure 10 shows a plot of the objective function  $F(\hat{\theta})$  vs. the penalty term  $\sum_{l=1}^n |\theta_l^{ref} - \theta_l|$ , for decreasing values of  $\lambda$ . As expected, while  $\lambda$  is decreased, the deviation of  $\hat{\theta}$

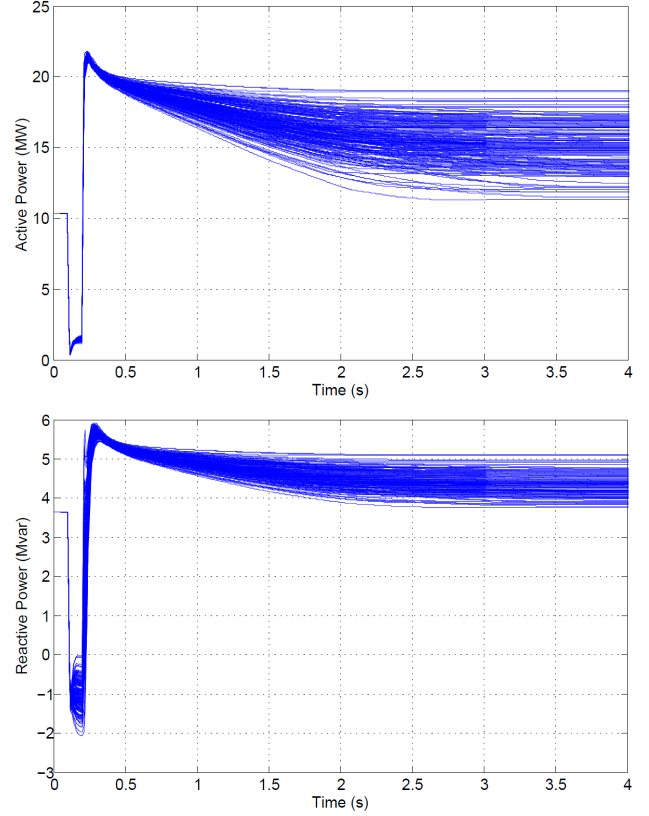


Fig. 9. Randomized evolutions of  $P$  and  $Q$  in response to disturbance # 13

with respect to  $\theta^{ref}$  increases, and  $F(\hat{\theta})$  decreases. At the point marked with a circle, corresponding to  $\lambda = 0.125$ , the accuracy criterion (5) is satisfied. The corresponding scores defined in (6),(7) are  $F_P^{max}(\hat{\theta}) = 0.77$  and  $F_Q^{max}(\hat{\theta}) = 0.97$ .

Figure 11 shows the relative differences defined in (11), for each of the 17 parameters. With a threshold  $\delta = 5\%$ , represented by the dashed red line, seven parameters are identified as non-significant. These are :

- for the aggregated load: the exponent  $\beta$  (see Fig. 1), the stator resistance, the magnetizing reactance and the inertia constant of the motor;
- for the aggregated IBG: no parameter discarded;
- for the equivalent impedances :  $R_a, R_b$  and  $X_a$  (which tends to confirm that the impedances estimated by network reduction were appropriate).

The validity of this approach has been verified as follows. The DE algorithm involving random changes of the variables, two separate executions may yield different values of  $\hat{\theta}$ . To assess this, the results of a set of separate executions of the DE algorithm have been compared, for the 17- and the 10-dimensional vectors  $\theta$ , respectively. In the former case, some components  $\theta_l$  exhibit significant variations, making comparisons difficult. With the 10-dimensional vector, a much lower variability has been observed, i.e. the variations from one DE execution to another are insignificant.

An illustration is provided in Fig. 12, showing 20 separate estimates of the  $V_Q$  component (see Fig. 2), when 17 and 10 components are included in  $\theta$ , respectively. It is clear that the

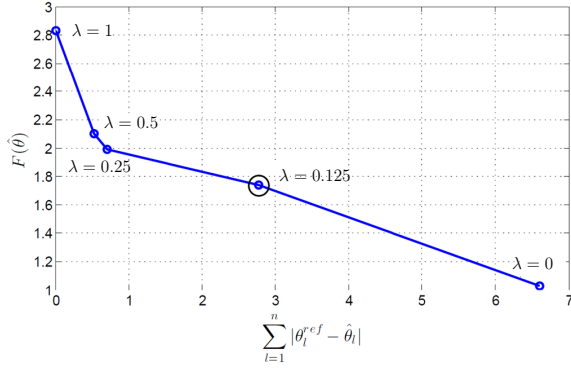


Fig. 10.  $F(\hat{\theta})$  vs.  $\sum_{l=1}^n |\theta_l^{ref} - \hat{\theta}_l|$  for decreasing values of  $\lambda$

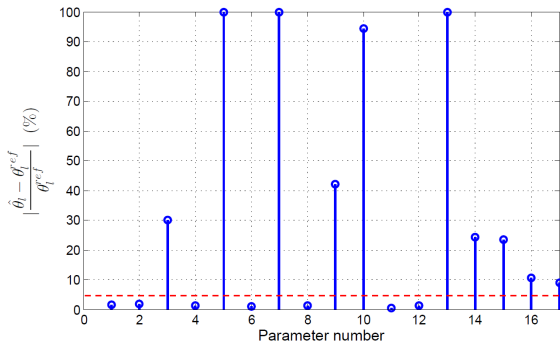


Fig. 11. LASSO method : final values of  $|\hat{\theta}_l - \theta_l^{ref}|/|\theta_l^{ref}|$  (in %)

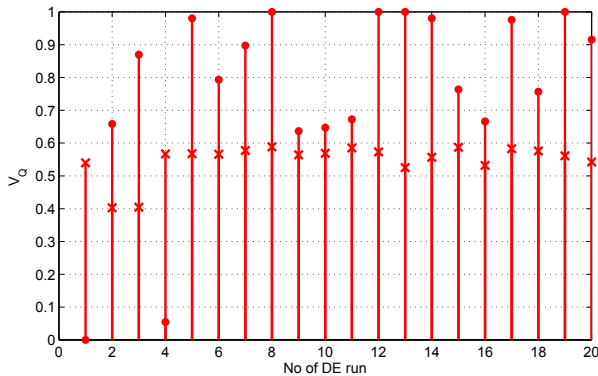


Fig. 12. Variability of  $V_Q$  estimates over 20 runs of the DE solver. Disks refer to the case with 17 components in  $\theta$ ; crosses refer to 10 components. The 20 values have been normalized so that the smallest is equal to 0 and the largest to 1

variability of the estimate from one run of DE to another is much smaller in the latter case. This yields a better model interpretation and consistency, which are expected advantages of a grey-box model.

### E. Step 2 : Optimizing the significant parameters

The recursive training iterations are shown in Table I. The  $c = 12$  candidate disturbances are the voltage dips No. 1 to 12 (see Fig. 5) not causing IBG disconnection. Columns 3 and

TABLE I  
RESULTS OF RECURSIVE TRAINING ALGORITHM

Iteration	Trained disturbances	trained disturbances		non trained disturbances	
		$F_P^{max}$	$F_Q^{max}$	$F_P^{max}$	$F_Q^{max}$
1	7, 8	0.78	0.96	1.57	2.34
2	7, 8, 11, 12	1.15	1.01	4.32	0.93
3	7, 8, 11, 12, 6	1.24	1.13	1.31	1.08
4	7, 8, 11, 12, 6, 2	1.29	1.21	0.79	0.87

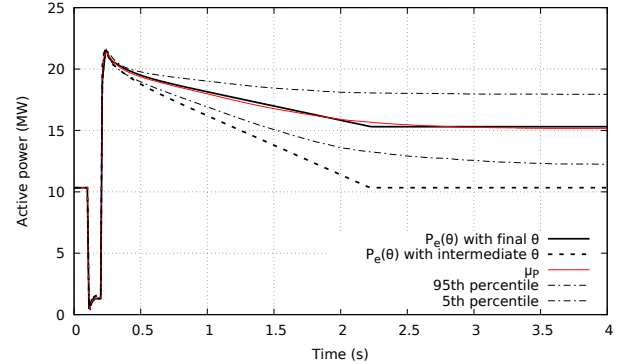


Fig. 13. Active power responses to the non-trained disturbance No 13

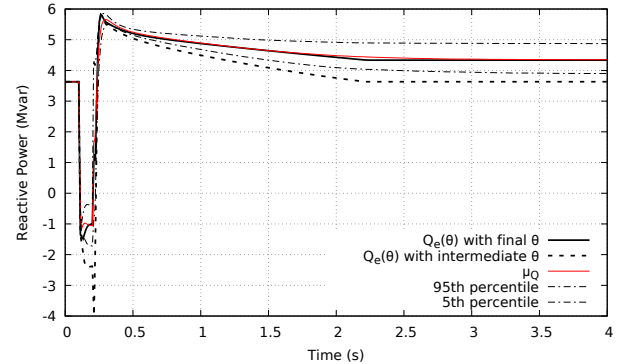


Fig. 14. Reactive power responses to the non-trained disturbance No 13

4 give the worst scores defined by (6),(7), while Columns 5 and 6 give the corresponding worst scores of the non-trained disturbances. After four iterations all non-trained disturbances show scores lower than the worst score of the trained ones, i.e. the stopping criterion (8), (9) is satisfied.

### F. Step 3 : Optimizing the partial tripping parameters

The algorithm execution continues now on the whole set of  $c = 14$  disturbances but focusing now on the value of  $\gamma$ ,  $V_{pt}$  and  $V_{ft}$  (see Fig. 4). This leads to adding one more training disturbance (No. 14, the most severe).

### G. Accuracy of the equivalent for non trained disturbances

In this section the accuracy of the equivalent is illustrated in response to disturbances *not used for its training*. Voltage dip No. 13 is considered, for which some IBGs disconnect. Figure 13 shows with dotted line the evolution of  $P_e$  for the intermediate  $\hat{\theta}$  obtained after Step 2. As  $\gamma$ ,  $V_{pt}$  and  $V_{ft}$

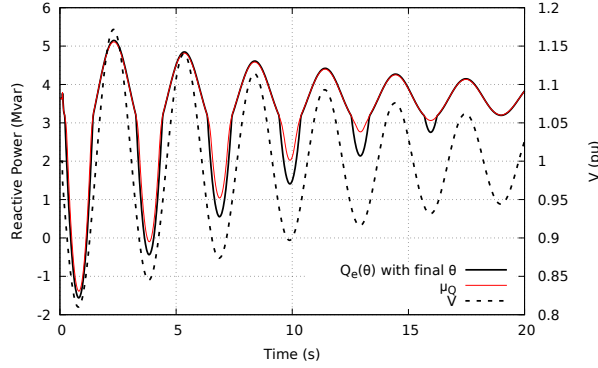


Fig. 15. Reactive power responses to an electromechanical oscillation

have not yet been optimized, IBG tripping is ignored and the response is inaccurate. On the other hand, the  $P_e$  response for the final  $\hat{\theta}$  obtained after Step 3 is shown with heavy solid line. It matches accurately the average response given by  $\mu_P$ , in particular its final value. For comparison purposes, Fig. 13 also shows the 5th and 95th percentiles, which reflect the dispersion of the randomized responses of unreduced system.

Similar curves relative to  $Q_e$  are given in Fig. 14. They confirm the accuracy of the equivalent for the reactive power.

#### H. Accuracy of the equivalent for other disturbances

Figure 15 shows the reactive power response of the equivalent to a very different (and also non-trained) disturbance, namely an oscillation of the magnitude and phase angle of  $\bar{V}_{tr}$  (see Fig. 3) that could represent the effect of an interarea electromechanical oscillation in the transmission system. The oscillation of the voltage magnitude is shown with dotted line. The other two curves show the evolution of respectively  $Q_e$  and  $\mu_Q$ . The latter has been obtained from randomized responses of the unreduced system to that disturbance. The overall accuracy is good, in particular near the first two nadirs. The discrepancies observed in the subsequent swings is due to a little excessive reactive current injection by the IBG in the equivalent (transiently decreasing the net reactive load).

Finally, Fig. 16 deals with a frequency transient, imposed by varying the phase angle of  $\bar{V}_{tr}$ . The frequency variation, which could result from a generator outage, is shown with dashed line. The other two curves show the evolutions of  $P_e$  and  $\mu_P$ , respectively. The latter has been obtained from randomized responses of the unreduced system. The accuracy of the equivalent is further confirmed by the perfect match of these two curves.

## VI. CONCLUSION

A methodology has been presented to identify ADN equivalents for use in transmission system dynamic simulations.

The proposed methodology is valid for any distribution systems. The procedure decomposes into the following steps:

- Monte-Carlo simulations are performed to account for parameter uncertainty in the unreduced ADN model. A set of randomized dynamic responses is thus generated for each disturbance;

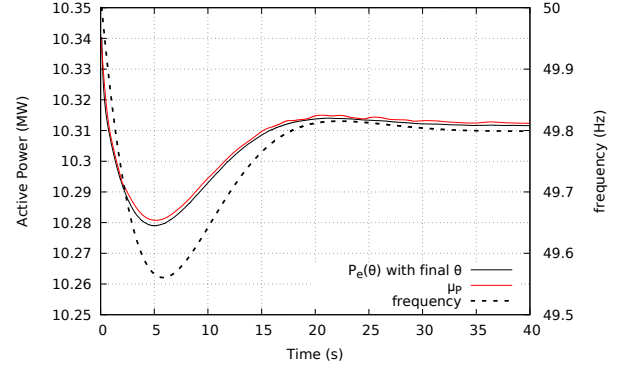


Fig. 16. Active power responses to a frequency transient

- a weighted least-square problem is solved to make the response of the equivalent approach the average of the randomized responses. The weights reflect the dispersion of the dynamic responses around their average;
- a metaheuristic (Differential Evolution) algorithm is used to deal with this minimization problem;
- for better interpretation of the results, a procedure based on the LASSO method allows removing from the identification the parameters with negligible impact on the response of the equivalent;
- multiple candidate disturbances are considered to avoid over-fitting only a few of them;
- a recursive procedure is used to involve the smallest possible sub-set of them in the least-square minimization;
- two sub-sets of parameters are estimated sequentially, using scenarios without and with IBG disconnection, respectively.

Simulation results show that the equivalent can reproduce the non-linear and discontinuous behaviour of the ADN, in particular the disconnection of some IBGs under low voltage conditions. The accuracy has been checked on disturbances not used for training, and illustrating a few applications.

The methodology presented in this paper has been recently extended to deal with different operating points. This entails: (i) selecting among a set of previously estimated  $\hat{\theta}$ 's the one that best fits the new operating point and, (ii) if none is satisfactory, adding a new estimate with minimal computational effort, which is another application of the LASSO method.

## APPENDIX A

### ALTERNATIVE STRUCTURES OF THE EQUIVALENT

A single equivalent IBG has been considered in this paper, but several of them can be used if the ADN hosts IBGs with different controls (e.g. small residential vs. large industrial PV units [13], [23]). A similar remark applies to loads.

A more general structure is shown in Fig. 17. Loads are split into residential and industrial. Moreover, IBGs are differentiated by grid requirements. Residential IBGs, such as rooftop PV units, are lumped separately; they have neither LVRT nor reactive current injection capabilities. An equivalent synchronous generator is also treated separately.

The chosen configuration should be in adequacy with the components. Configurations such as that of Fig. 17 are recommended in [26], encouraging to differentiate the aggregated

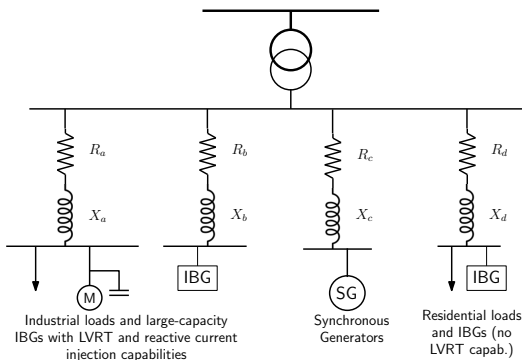


Fig. 17. A more general structure of the equivalent

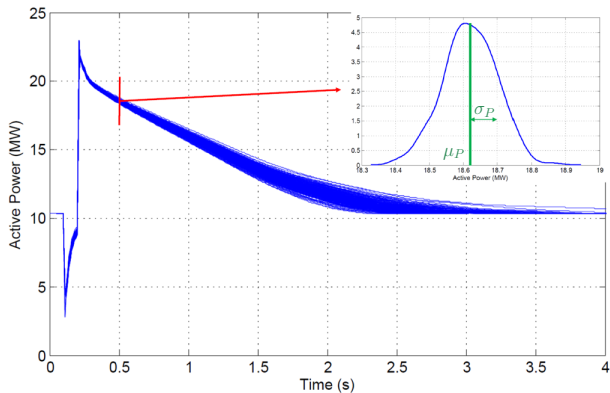


Fig. 18. Gaussian randomized parameters:  $P$  and  $Q$  responses to dist. # 7

distributed energy resources according to performance requirements, to represent the fundamentally different behavior of future and legacy units, respectively.

## APPENDIX B

### MC SIMULATIONS OF UNREDUCED SYSTEM WITH GAUSSIAN RANDOMIZED PARAMETERS

MC simulations with randomized parameters obeying a Gaussian, instead of a uniform distribution are reported here. For coherency between the two cases, the Gaussian distribution of parameter  $p_i$  has its average set to  $(p_i^{min} + p_i^{max})/2$  and its standard deviation to  $(p_i^{max} - p_i^{min})/6$ , where  $p_i^{min}$

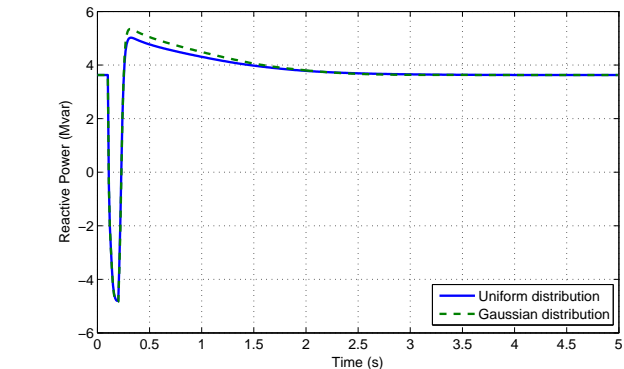
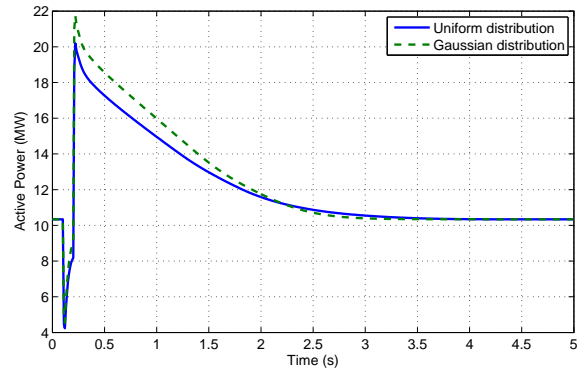


Fig. 19. Evolutions of  $\mu_P$  and  $\mu_Q$  for uniform and Gaussian distributions of the parameters; disturbance # 7

(resp.  $p_i^{max}$ ) is the lower (resp. upper) bound of the uniform distribution.

Figure 18 shows the randomized evolutions of the active power  $P$  and reactive power  $Q$  in response to disturbance No. 7. The curves can be compared with those in Fig. 8. As expected, the responses are significantly less dispersed. The distributions of  $P$  and  $Q$  values at  $t = 0.5$  s are closer to Gaussian ones.

Figure 19 shows, for the same disturbance, the evolution of  $\mu_P$  and  $\mu_Q$  for a uniform and a Gaussian distribution of parameters, respectively. The difference is marginal. Figure 20 shows the corresponding evolutions of  $\sigma_P$  and  $\sigma_Q$ . The difference between both distributions is pronounced over a 2-second time interval after the recovery of voltage. The Gaussian distribution yields smaller  $\sigma_P$  and  $\sigma_Q$  values, which confirms the smaller dispersion of the power responses.

All in all, whether the parameter distribution is Gaussian or uniform influences only marginally the reference evolution that the equivalent must approach. The difference lies in the weighting factors assigned to the various points in time. However, as many of the points tend to have a higher weight with the Gaussian distribution, the resulting estimate  $\hat{\theta}$  is only marginally affected.

## REFERENCES

- [1] B. Zaker, G. B. Gharehpetian and M. Karrari, "A Novel Measurement-Based Dynamic Equivalent Model of Grid-Connected Microgrids," *IEEE Trans. on Industrial Informatics*, vol. 15, no. 4, 2019.

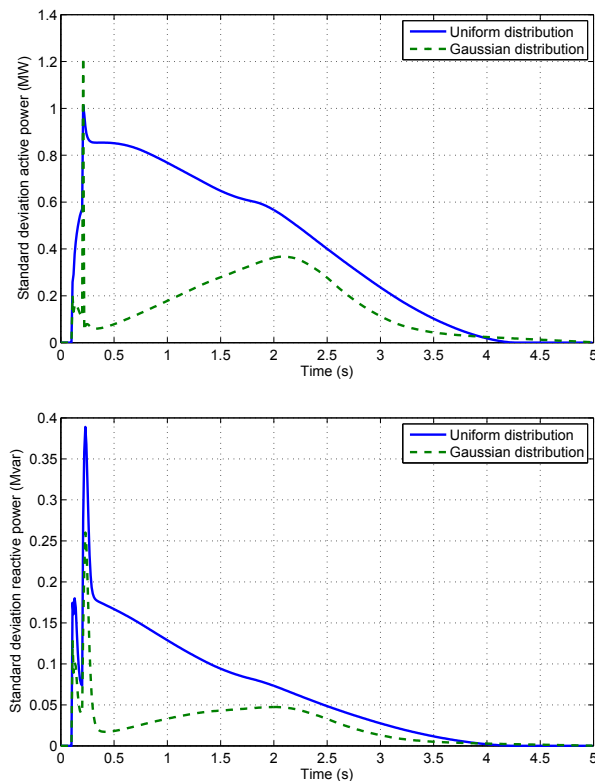


Fig. 20. Evolutions of  $\sigma_P$  and  $\sigma_Q$  for uniform and Gaussian distributions of the parameters; disturbance # 7

- [2] C. Zheng, S. Wang, Y. Liu, C. Liu, W. Xi, C. Fang and S. Liu, "A Novel Equivalent Model of Active Distribution Networks Based on LSTM," *IEEE Trans. on Neural Networks and Learning Systems*, vol. 30, no. 9, pp. 2611-2624, Sept. 2019.
- [3] E. O. Kontis, T. A. Papadopoulos, M. H. Syed, E. Guillo-Sansano, G. M. Burt and G. K. Papagiannis, "Artificial-Intelligence Method for the Derivation of Generic Aggregated Dynamic Equivalent Models," *IEEE Trans. on Power Systems*, vol. 34, no. 4, pp. 2947-2956, July 2019.
- [4] C.W. Taylor, *Power System Voltage Stability*. Mc Graw Hill, EPRI Power Engineering Series, 1994.
- [5] IEEE Standards Coordinating Committee 21, "IEEE Standard for Interconnection and Interoperability of Distributed Energy Resources with Associated Electric Power Systems Interfaces," Approved 15 February, 2018.
- [6] "Commission Regulation (EU) 2016/631 of 14 April 2016 establishing a network code on requirements for grid connection of generators," pp. 1-68, 27 April 2016. Available: [https://www.entsoe.eu/network\\_codes/rfg/](https://www.entsoe.eu/network_codes/rfg/). [Accessed October 2019].
- [7] C. Robert and G. Casella, *Monte Carlo Statistical Methods*. Springer Science & Business Media, 2013.
- [8] G. Chaspierre, P. Panciatici and T. Van Cutsem, "Modelling Active Distribution Networks under Uncertainty: Extracting Parameter Sets from Randomized Dynamic Responses," *Proc. 20th PSCC conference*, Dublin (Ireland), 2018.
- [9] A. Arif, Z. Wang, J. Wang, B. Mather, H. Bashualdo and D. Zhao, "Load modeling. A review," *IEEE Transactions on Smart Grid*, vol. 9, no. 6, pp. 5986-5999, 2017.
- [10] J. Milanović (Convener), "Modelling and aggregation of loads in flexible power networks," *Report of CIGRE WG C4.605*, 2014.
- [11] N. Hatziaiyriou (Convener), "Contribution to Bulk System Control and Stability by Distributed Energy Resources connected at Distribution Network," *IEEE PES Tech. Report PES-TR22*, 2017.
- [12] F. Conte, F.D' Agostino, S. Massucco, G. Palombo, F. Silvestro, C. Bossi and M. Cabiati "Dynamic Equivalent Modelling of Active Distribution Networks for TSO-DSO Interactions," *Proc. IEEE ISGT Europe conference*, Torino (Italy), 2017.
- [13] G. Chaspierre, P. Panciatici and T. Van Cutsem, "Aggregated Dynamic Equivalent of a Distribution System hosting Inverter-based Generators," *Proc. 20th PSCC conference*, Dublin (Ireland), 2018.
- [14] X. Wu, X. Lei, Y. Lan, A. Monti and F. Gao, "A New Dynamic Equivalent of Active Distribution Network for Transient Analysis," *2018 International Conference on Power System Technology (POWERCON)*, pp. 529-536, Guangzhou, 2018.
- [15] F. Conte, F. D'Agostino and F. Silvestro, "Operational constrained nonlinear modeling and identification of active distribution networks," *Electric Power Systems Research*, vol. 168, pp 92-104, 2019.
- [16] X. Shang, Z. Li, J. Zheng, Q.H. Wu, "Equivalent modeling of active distribution network considering the spatial uncertainty of renewable energy resources," *Electrical Power and Energy Systems*, vol. 112, pp. 83-91, 2019.
- [17] N. Fulgencio, C. Moreira, L. Carvalho and J. P. Lopes, "Aggregated dynamic model of active distribution networks for large voltage disturbances," *Electric Power Systems Research*, vol. 178, pp.1-13, 2020.
- [18] P. Kundur, *Power system stability and control*, McGraw-hill New York, 1994.
- [19] L. Ljung, *System identification: theory for the user*. PTR Prentice Hall, Upper Saddle River, NJ, 1999.
- [20] R. Tibshirani, "Regression shrinkage and selection via the LASSO," *Journal of the Royal Statistical Society. Series B*, vol. 58, no. 1, pp. 267-288, 1996.
- [21] M. Rasouli, D.T. Westwick and W.D. Rosehart, "Reducing induction motor identified parameters using a nonlinear LASSO method," *Electric Power Systems Research*, vol. 88, pp. 1-8, 2012.
- [22] M. Rasouli and C. Lagoa, "A nonlinear term selection method for improving synchronous machine parameters estimation," *International Journal of Electrical Power & Energy Systems*, vol. 85, pp. 77-86, 2017.
- [23] G. Chaspierre, G. Denis, P. Panciatici and T. Van Cutsem, "Dynamic equivalent of an active distribution network taking into account model uncertainties," *Proc. 13th IEEE PES PowerTech conf.*, Milan (Italy), 2019.
- [24] G. Chaspierre, P. Panciatici and T. Van Cutsem, "Dynamic Equivalent of a Distribution Grid Hosting Dispersed Photovoltaic Units," *Proc. IREP'17 Symposium*, Espinho (Portugal), 2017.
- [25] B. Weise, "Impact of k-factor and active current reduction during fault-ride-through of generating units connected via voltage-sourced converters on power system stability," *IET Renewable Power Generation*, vol. 9, no. 1, pp. 25-36, 2015.
- [26] North American Electric Reliability Corporation (NERC), "Distributed Energy Resources Connection Modeling and Reliability Considerations," February, 2017.
- [27] P. Pourbeik, J. Weber, D. Ramasubramanian, J. Sanchez-Gasca, J. Senthil, P. Zadhast, J. C Boemer, A. Gaikwad, I. Green, S. Tacke, R. Favela, S. Wang, S. Zhu and M. Torgesen, "An aggregate dynamic model for distributed energy resources for power system stability studies," *Cigre Science & Engineering*, no. 14, pp. 38-48, June 2019.
- [28] K.V. Price, R.M. Storm and J.A. Lampinen, *Differential Evolution - A Practical Approach to Global Optimization*, Springer, 2005.
- [29] J. Vesterstrom and T. Rene, "A Comparative Study of Differential Evolution, Particle Swarm Optimization, and Evolutionary Algorithms on Numerical Benchmark Problems," *Proc. of the IEEE 2004 Congress on Evolutionary Computation*, pp. 1980-1987, 2004.
- [30] V. Miranda and N. Fonseca, "EPSO - best-of-two-worlds meta-heuristic applied to power system problems," *Proc. of the 2002 Congress on Evolutionary Computation. CEC'02 (Cat. No.02TH8600)*, Honolulu, HI, USA, 2002, pp. 1080-1085 vol.2.
- [31] V. Miranda and R. Alves, "Differential Evolutionary Particle Swarm Optimization (DEEPSO): A Successful Hybrid," *2013 BRICS Congress on Computational Intelligence and 11th Brazilian Congress on Computational Intelligence*, Ipojuca, 2013, pp. 368-374.
- [32] J. Yang, J. Zhang and W. Pan, "Dynamic equivalents of power system based on extended two Particle Swarm Optimization," *Third International Conference on Natural Computation (ICNC 2007)*. IEEE, vol. 5, pp. 609-613, 2007.
- [33] D. Gusain, J.L. Rueda, J.C. Boemer and P. Palensky, "Identification of Dynamic Equivalents of Active Distribution Networks through MVMO," *IFAC-PapersOnline*, vol. 49, no. 27, pp. 262-267, 2016.
- [34] P.R. Mier, "A tutorial on Differential Evolution with Python," Toulouse (France), September 05, 2017. Available: <https://pablormier.github.io/2017/09/05/a-tutorial-on-differential-evolution-with-python/> [Accessed September, 2018].
- [35] P. Aristidou, D. Fabozzi and T. Van Cutsem, "Dynamic simulation of large-scale power systems using a parallel Schur-complement-based decomposition method," *IEEE Trans. on Parallel and Distributed Systems*, vol. 25, no. 10, pp. 2561-2570, 2014.